PHYSICAL REVIEW B **95**, 045134 (2017)

Exchange couplings for Mn ions in CdTe: Validity of spin models for dilute magnetic II-VI semiconductors

Thorben Linneweber,[1] Jörg Bünemann,[2] Ute Löw,[1] Florian Gebhard,[3] and Frithjof Anders[1]
[1]*Lehrstuhl für Theoretische Physik II, Technische Universität Dortmund, D-44227 Dortmund, Germany*
[2]*Institut für Physik, BTU Cottbus-Senftenberg, D-03013 Cottbus, Germany*
[3]*Fachbereich Physik, Philipps-Universität Marburg, D-35032 Marburg, Germany*

(Received 7 July 2016; revised manuscript received 3 November 2016; published 23 January 2017)

We employ density-functional theory (DFT) in the generalized gradient approximation (GGA) and its extensions GGA+U and GGA+Gutzwiller to calculate the magnetic exchange couplings between pairs of Mn ions substituting Cd in a CdTe crystal at very small doping. DFT(GGA) overestimates the exchange couplings by a factor of 3 because it underestimates the charge-transfer gap in Mn-doped II-VI semiconductors. Fixing the nearest-neighbor coupling J_1 to its experimental value in GGA+U, in GGA+Gutzwiller, or by a simple scaling of the DFT(GGA) results provides acceptable values for the exchange couplings at second-, third-, and fourth-neighbor distances in Cd(Mn)Te, Zn(Mn)Te, Zn(Mn)Se, and Zn(Mn)S. In particular, we recover the experimentally observed relation $J_4 > J_2, J_3$. The filling of the Mn 3d shell is not integer, which puts the underlying Heisenberg description into question. However, using a few-ion toy model the picture of a slightly extended local moment emerges so that an integer 3d-shell filling is not a prerequisite for equidistant magnetization plateaus, as seen in experiment.

DOI: 10.1103/PhysRevB.95.045134

I. INTRODUCTION

The introduction of spin degrees of freedom in semiconductors leads to a variety of new phenomena, e.g., giant Zeeman splitting or giant Faraday rotation [1–3]; for recent studies of spin diffusion and spin relaxation of Mn-doped semiconductor heterostructures, see Refs. [4,5] and references therein. Over the last decades, the field of diluted magnetic semiconductors has attracted a lot of attention with the perspective of using the spin degree of freedom for electronic devices ("spintronics") [6–9]. Apart from potential applications, the description of magnetic ions in a semiconducting host material poses an interesting but difficult problem in theoretical condensed-matter physics.

Mn-doped II-VI semiconductors were among the first diluted magnetic semiconductors to be studied intensively [1,2]. For small doping in CdTe, the isovalent Mn ions replace the Cd ions. Early on, it was pointed out that the Mn ions possess magnetic moments the couplings of which are mediated by the semiconductor host material. The observation of equidistant magnetization steps confirmed the assumption that the Mn ions carry spin $s = 5/2$ and their mutual interaction can be expressed in terms of a Heisenberg model with antiferromagnetic pair couplings $J_n > 0$ at nth-neighbor distance [10–14].

Not only the exchange couplings between nearest neighbors but also those between Mn ions at second-, third-, and fourth-neighbor distances were experimentally determined; all other couplings are negligibly small, $J_{n\geqslant 5} \ll J_4$. A modeling of the magnetization curves at very low temperatures leads to the surprising result that $J_4 > J_2, J_3$ [12,13], i.e., the exchange couplings do not decay monotonously as a function of the geometrical distance.

The unexpected nonmonotonous decay of J_n as a function of the Mn-Mn separation, and also the overall size of the exchange couplings, are unexplained. Only the nearest-neighbor exchange couplings J_1 for Mn-doped II-VI semiconductors were calculated using the superexchange approach [15–18], or density-functional theory (DFT) in the local-density approximation, DFT (LSDA), and in DFT(LSDA)+U [19,20].

In this work, we calculate the exchange couplings $J_{n\leqslant 4}$ using three itinerant-electron approaches: (i) the generalized-gradient approximation (GGA) to DFT with the functional of Perdew, Burke, and Ernzerhof [21]; (ii) GGA+U as implemented in the FLEUR package [22]; and (iii) GGA+Gutzwiller for a suitable two-ion Hubbard model. We confirm that $J_4 > J_2, J_3$ and find a reasonable agreement with measured values for Cd(Mn)Te, Zn(Mn)Te, Zn(Mn)Se, and Zn(Mn)S. Furthermore, our analysis shows that the filling of the Mn 3d shell is not integer, which challenges the notion of Mn ions carrying a spin $s = 5/2$. We study a few-ion toy model to show that the noninteger filling remains consistent with equidistant magnetization plateaus. The picture of a spatially distributed spin $s = 5/2$ emerges which includes the neighboring Wannier orbitals that hybridize with the Mn 3d states. We therefore conclude that the concept of interacting Heisenberg spins remains applicable for Mn ions diluted in II-VI semiconductors.

Our paper is organized as follows. In Sec. II we specify the setup for our DFT(GGA) and GGA+U calculations. Moreover, we derive the two-ion Hubbard model for our GGA+Gutzwiller approach, and define the exchange couplings in terms of ground-state energy differences of the itinerant electron description. In Sec. III we provide the exchange couplings for up to fourth neighbors in Cd(Mn)Te, Zn(Mn)Te, Zn(Mn)Se, and Zn(Mn)S, and compare them to experiment. As an example, we discuss the magnetization as a function of magnetic field for $Cd_{1-x}Mn_xTe$ for very low doping, $x = 0.005$. In Sec. IV we discuss the magnetization curve for a few-ion toy model and show that equidistant magnetization plateaus can be observed even though the filling of the Mn 3d shell is not integer. Short conclusions, Sec. V, close our presentation.

II. ION PAIRS IN A SEMICONDUCTOR HOST

We are interested in the properties of manganese atoms diluted in a II-VI host semiconductor at low temperatures and in sizable magnetic fields. To be definite, we shall focus on CdTe. For very small Mn concentrations x in $\mathrm{Cd}_{1-x}\mathrm{Mn}_x\mathrm{Te}$, we may safely assume that the Mn^{2+} ions substitute the isovalent Cd^{2+} ions. We tested that it is a reasonable approximation to neglect lattice distortions in the theoretical analysis because structural relaxations turned out to be small within the DFT(GGA) calculations.

CdTe crystallizes in the zinc-blende ($\beta-\mathrm{ZnS}$) structure where the fcc lattice of the Te ions is shifted against the fcc lattice of the Cd ions by $a/4$ along the diagonal of the cubic cell of length $a = 6.482$ Å [23]. Figure 1(a) shows a fcc unit cell with one Mn atom replacing one out of four Cd atoms ($x = 0.25$).

The spin of an isolated Mn ion aligns with any finite magnetic field. The nontrivial magnetization curves (deviating from a Brillouin function) seen in experiment [13] are due to the exchange interaction between different Mn ions. Test calculations confirmed that the interaction of three or more Mn ions is given by the sum of pair interactions so that we can concentrate on the interaction between pairs of Mn ions as a function of their distance. We found in numerically expensive Gutzwiller calculations with $L = 512$ atoms in the unit cell that the interaction between two Mn ions beyond fourth-neighbor distance is negligibly small. In Fig. 1(b) we show the first, second, third, and fourth neighbors on the fcc sublattice in CdTe.

A. GGA and GGA+U calculations

Ideally, we should study a single pair of Mn ions with Cd ions on all other sites of the cation fcc lattice. However, practical band-structure calculations require translational symmetry. Therefore, we start from large but finite cells with L atoms that contain two Mn ions, and link them together so that periodic boundary conditions apply in all three spatial directions. Modern band-structure program packages permit the investigation of large cells (“supercells”). In this paper, we use supercells with $L = 128$ atoms, which are obtained by transforming the eight-atomic unit cell shown in Fig. 1 by the matrix (022/202/220). This supercell is sufficient to study Mn pairs that are maximally fourth-nearest neighbors.

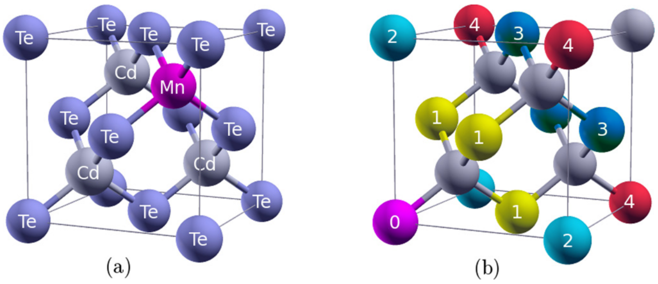

FIG. 1. (a) Zn-blende structure for $\mathrm{Cd}_{0.75}\mathrm{Mn}_{0.25}\mathrm{Te}$ where one out of four Cd atoms is replaced by a Mn atom. (b) Positions of first, second, third, and fourth neighbors on the Cd fcc sublattice from the Cd atom in the lower left corner.

For our investigations we use the FLEUR package [22], a high-precision implementation of the full potential linearized augmented plane-wave (FLAPW) approach to DFT in the GGA. The program package FLEUR also offers the option to include the effect of the correlations between the electrons in the partly filled $3d$ shell of the Mn ions on a mean-field level (GGA+U). In Sec. III, we compile results for the Mn-Mn interaction from both band-structure approaches.

We run the FLEUR code using the following settings. We use the GGA functional of Perdew, Burke, and Ernzerhof [21] for the exchange-correlation energy. Since we are investigating a band insulator with a sizable gap, it is sufficient to use only ten inequivalent **k** points in the irreducible part of the Brillouin zone; depending on the impurity positions, this corresponds to 20 or 40 **k** points in the full Brillouin zone. The basis functions inside the muffin tins are expanded in spherical harmonic functions with a cutoff of $L_{\max} = 10$. The muffin tin radii are $R_{\mathrm{Cd}} = R_{\mathrm{Mn}} = 2.64$ a.u. and $R_{\mathrm{Te}} = 2.58$ a.u. (1 atomic unit $= a_{\mathrm{B}} = 0.529$ Å). We use $R_{\mathrm{Te}}K_{\max} = 8.26$, where $K_{\max}$ is the plane-wave cutoff. For the GGA+U calculations we use the standard double-counting correction [24]. Due to the computational cost of the DFT calculations a rigourous analysis of the error in the coupling constants (see Sec. II C) is not feasible. However, for testing purposes, we also calculated J_1 and J_4 for CdTe with (i) 20 inequivalent **k** points and (ii) a larger plane-wave cutoff of $R_{\mathrm{Te}}K_{\max} = 9.29$. The results for J_1 and J_4 in these calculations change by less than 1%.

B. GGA+Gutzwiller approach

The electrons in the Mn ions’ $3d$ shell are strongly correlated. Therefore, more sophisticated many-particle techniques should be employed. For example, it would be desirable to use the fully self-consistent Gutzwiller-DFT [25–27]. At present, however, the required large unit cells prevent us from doing such a calculation and we restrict ourselves to a less costly method that is based on the evaluation of a Gutzwiller wave function for a tight-binding model with Hubbard-type interactions on the two Mn sites.

1. Derivation of the two-ion Hubbard model

The code WANNIER90 permits a downfolding of the band structure to a tight-binding Hamiltonian in position space [28]. We project onto a basis of s orbitals and p orbitals for each of the semiconductor atoms and s, p, and d orbitals for the Mn impurity. However, the downfolding procedure is limited to $L = 16$ atoms in the unit cell so that we cannot derive the tight-binding model for a pair of Mn ions directly.

To overcome this limitation, we assume that the combined influence of two Mn ions on the electron transfer between two lattice sites can be approximated by the linear superposition of the influence of two individual Mn ions. Under this linearity assumption, we are left with the investigation of a single Mn ion in a CdTe supercell of $L = 16$ atoms, obtained by transforming the eight-atomic unit cell shown in Fig. 1 by the matrix (011/101/110). For our GGA calculations we use 120 **k** points in the irreducible part of the Brillouin zone (1/24 of the full Brillouin zone) and $R_{\mathrm{Te}}K_{\max} = 9.80$.

First, we calculate the band structure for pure CdTe. The downfolding provides the tight-binding Hamiltonian for CdTe,

$$\hat{H}^{\mathrm{CdTe}} = \sum_{\mathbf{i},\mathbf{j},b_1,b_2,\sigma} t^{\mathbf{j},b_2,\sigma}_{\mathbf{i},b_1,\sigma}\,\hat{c}^{\dagger}_{\mathbf{i},b_1\sigma}\hat{c}_{\mathbf{j},b_2\sigma}, \tag{1}$$

where $\hat{c}^{\dagger}_{\mathbf{i},b\sigma}$ ($\hat{c}_{\mathbf{i},b\sigma}$) creates (annihilates) an electron in the orbital b with spin $\sigma = \uparrow,\downarrow$. Due to the symmetry of our crystal, there are no local hybridization terms, and we may write

$$\begin{aligned}\hat{H}^{\mathrm{CdTe}} &= \hat{T}^{\mathrm{CdTe}} + \hat{V}^{\mathrm{CdTe}},\\ \hat{T}^{\mathrm{CdTe}} &= \sum_{\mathbf{i}\neq\mathbf{j},b_1,b_2,\sigma} t^{\mathbf{j},b_2,\sigma}_{\mathbf{i},b_1,\sigma}\,\hat{c}^{\dagger}_{\mathbf{i},b_1\sigma}\hat{c}_{\mathbf{j},b_2\sigma},\\ \hat{V}^{\mathrm{CdTe}} &= \sum_{\mathbf{i},b,\sigma} t^{\mathbf{i},b,\sigma}_{\mathbf{i},b,\sigma}\,\hat{n}_{\mathbf{i},b\sigma},\end{aligned} \tag{2}$$

where $\hat{n}_{\mathbf{i},b\sigma} = \hat{c}^{\dagger}_{\mathbf{i},b\sigma}\hat{c}_{\mathbf{i},b\sigma}$ counts the number of electrons with spin σ in orbital b on site $\mathbf{i}$.

Next, we repeat the paramagnetic calculation with a single Mn ion at position $\mathbf{f}$ which leads to a new set of electron transfer matrix elements $(t^{\mathbf{j},b_2,\sigma_2}_{\mathbf{i},b_1,\sigma_1})^{\mathbf{f}}$

$$\hat{H}^{\mathrm{CdTe},\mathbf{f}} = \sum_{\mathbf{i}\neq\mathbf{j},b_1,b_2,\sigma} \left(t^{\mathbf{j},b_2,\sigma}_{\mathbf{i},b_1,\sigma}\right)^{\mathbf{f}}\hat{c}^{\dagger}_{\mathbf{i},b_1\sigma}\hat{c}_{\mathbf{j},b_2\sigma} + \hat{V}^{\mathrm{CdTe}}. \tag{3}$$

Due to periodic boundary conditions and the translational invariance of the crystal, the bands for CdTe with a single Mn ion do not depend on $\mathbf{f}$. The corresponding bands for pure CdTe and with a single Mn ion in the $L = 16$ supercell are shown in Fig. 2.

The upper part of the figure shows that the direct gap at the Γ point is $E_{\mathrm{sp}} = 0.76\,\mathrm{eV}$, in agreement with previous calculations [29]. However, DFT(LDA) and DFT(GGA) underestimate the gap for the insulator CdTe. The (exciton) gap, a lower bound on the single-particle gap, is found at $E_{\mathrm{xc}} = 1.5\,\mathrm{eV}$ for CdTe [30]. DFT(GGA) also underestimates the charge-transfer gap in Mn-doped II-VI semiconductors between Te and Mn levels so that the resulting exchange couplings are too large (see Sec. III A 1). The origin of the exchange coupling can be inferred from the lower part of Fig. 2. The Mn $3d$ bands are grouped around the Fermi energy so that they push down the CdTe bands that were below the gap, and hybridize at the Γ point with a dominant Te band above the CdTe gap. The band structure shows that the Mn-Te hybridization is responsible for the interaction between Mn ions.

To set up our Hamiltonian in the presence of two Mn impurities, we define the corrections to the electron transfer amplitudes

$$\left(\Delta^{\mathbf{j},b_2,\sigma}_{\mathbf{i},b_1,\sigma}\right)^{\mathbf{f}} = \left(t^{\mathbf{j},b_2,\sigma}_{\mathbf{i},b_1,\sigma}\right)^{\mathbf{f}} - t^{\mathbf{j},b_2,\sigma}_{\mathbf{i},b_1,\sigma}. \tag{4}$$

According to our linear superposition scheme, we model the presence of a second Mn impurity in our tight-binding Hamiltonian by adding independently the corrections for the first Mn ion at site $\mathbf{f}_1$ and the second impurity at site $\mathbf{f}_2$. This defines our tight-binding Hamiltonian for the two-site problem

$$\begin{aligned}\hat{H}^{\mathrm{tb}} &= \sum_{\mathbf{i}\neq\mathbf{j},b_1,b_2,\sigma} \left(t^{\mathbf{j},b_2,\sigma}_{\mathbf{i},b_1,\sigma}\right)^{\mathbf{f}_1,\mathbf{f}_2}\hat{c}^{\dagger}_{\mathbf{i},b_1\sigma}\hat{c}_{\mathbf{j},b_2\sigma} + \hat{V}^{\mathrm{CdTe}},\\ \left(t^{\mathbf{j},b_2,\sigma}_{\mathbf{i},b_1,\sigma}\right)^{\mathbf{f}_1,\mathbf{f}_2} &= \left(\Delta^{\mathbf{j},b_2,\sigma}_{\mathbf{i},b_1,\sigma}\right)^{\mathbf{f}_1} + \left(\Delta^{\mathbf{j},b_2,\sigma}_{\mathbf{i},b_1,\sigma}\right)^{\mathbf{f}_2} + t^{\mathbf{j},b_2,\sigma}_{\mathbf{i},b_1,\sigma}.\end{aligned} \tag{5}$$

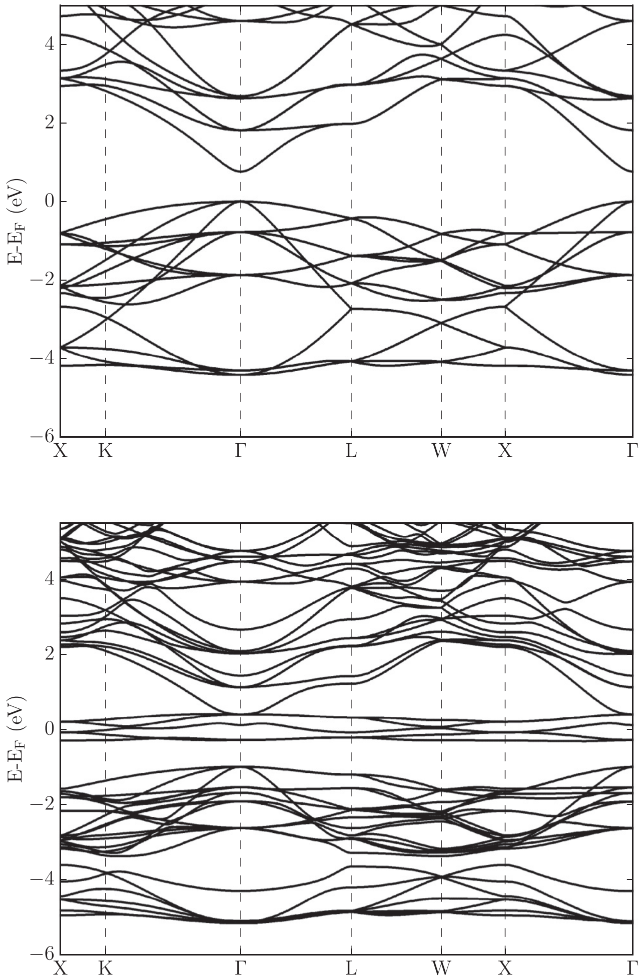

FIG. 2. Band structures of CdTe (upper part of the figure) and of $\mathrm{Cd}_{0.875}\mathrm{Mn}_{0.125}\mathrm{Te}$ (lower part of the figure), calculated from a supercell with $L = 16$ atoms without (with) a single Mn atom in the supercell using the FLEUR program package.

Our approximation neglects the joint influence of the impurities on the electron transfer-matrix elements in their surrounding, in the spirit of standard alloy theory [31]. The supercells for the two-ion Hubbard model can be much larger than those used for its construction ($L = 16$). For our further Gutzwiller calculations we work with cells containing $L = 512$ atoms.

As a last step, we add the Hubbard interaction on the two Mn sites $\mathbf{f}_1$ and $\mathbf{f}_2$ and obtain the two-ion Hubbard model

$$\begin{aligned}\hat{H} &= \hat{H}^{\mathrm{tb}} + \hat{H}^{\mathrm{loc}}_{\mathbf{f}_1} + \hat{H}^{\mathrm{loc}}_{\mathbf{f}_2} + \hat{H}^{\mathrm{dc}},\\ \hat{H}^{\mathrm{loc}}_{\mathbf{g}} &= \sum_{c_1,\ldots,c_4=1}^{5}\;\sum_{\sigma,\sigma'=\uparrow,\downarrow} U^{(c_1\sigma),(c_2\sigma')}_{(c_3\sigma'),(c_4\sigma)}\\ &\quad\times \hat{c}^{\dagger}_{\mathbf{g},c_1\sigma}\hat{c}^{\dagger}_{\mathbf{g},c_2\sigma'}\hat{c}_{\mathbf{g},c_3\sigma'}\hat{c}_{\mathbf{g},c_4\sigma},\\ \hat{H}^{\mathrm{dc}} &= -E_{\mathrm{dc}}(\hat{n}_{\mathbf{f}_1} + \hat{n}_{\mathbf{f}_2}).\end{aligned} \tag{6}$$

Here, $U^{\cdots}_{\cdots}$ describes the Coulomb interaction between the electrons in the $3d$ shell in the ten spin-orbit level $(c_l\sigma_l)$ in either of the two Mn ions. Using some simplifying assumptions, all interaction coefficients can be expressed in terms of an intraorbital Hubbard U and an interorbital Hund's-rule J [25] (see Sec. III).

Lastly, $\hat{H}^{\mathrm{dc}}$ accounts for the double counting of interaction terms between the $3d$ electrons on a mean-field level, where $\hat{n}_{\mathbf{g}} = \sum_{c,\sigma} \hat{n}_{\mathbf{g},c\sigma}$ counts the number of correlated electrons on the Mn site $\mathbf{g}$. We use a particularly simple form for the double-counting term. In essence, the choice of E_{dc} permits us to fix the average number of electrons in the correlated Mn $3d$ orbitals and we shall present our results as a function of $n_d \equiv \sum_{c,\sigma} \langle n_{\mathbf{f}_1,c,\sigma}\rangle = \sum_{c,\sigma}\langle n_{\mathbf{f}_2,c,\sigma}\rangle$. Typically, we need $E_{\mathrm{dc}} \approx 20\,\mathrm{eV}$ to adjust $n_d \approx 5$.

2. Gutzwiller variational state

We approximate the true ground state of our model Hamiltonian (6) by a Gutzwiller variational state,

$$|\Psi_{\mathrm{G}}\rangle = \hat{P}_{\mathbf{f}_1}\hat{P}_{\mathbf{f}_2}|\Phi_0\rangle, \tag{7}$$

where $|\Phi_0\rangle$ is the ground state of an (effective) single-particle Hamiltonian H_0^{qp}, and $\hat{P}_{\mathbf{g}}$ is the single-site Gutzwiller correlator,

$$\hat{P}_{\mathbf{g}} = \sum_{\Gamma} \lambda_{\Gamma}\hat{m}_{\mathbf{g},\Gamma}, \tag{8}$$

with $\mathbf{g} = \mathbf{f}_1,\mathbf{f}_2$. Here, $\hat{m}_{\mathbf{g},\Gamma} = |\Gamma\rangle_{\mathbf{gg}}\langle\Gamma|$ projects onto the atomic eigenstate $|\Gamma\rangle_{\mathbf{g}}$ of $\hat{H}^{\mathrm{loc}}_{\mathbf{g}} = \sum_{\Gamma} E_{\Gamma}\hat{m}_{\mathbf{g},\Gamma}$, and λ_{Γ} are real variational parameters for each of the $2^{10} = 1024$ states in the Mn $3d$ shell.

3. Gutzwiller approximation and energy minimization

To obtain the optimal values of the variational parameters λ_{Γ} and the optimal single-particle product state $|\Phi_0\rangle$, we must minimize the energy functional

$$E^{\mathrm{var}}(\{\lambda_{\Gamma},|\Phi_0\rangle\}) = \frac{\langle\Psi_{\mathrm{G}}|\hat{H}|\Psi_{\mathrm{G}}\rangle}{\langle\Psi_{\mathrm{G}}|\Psi_{\mathrm{G}}\rangle}. \tag{9}$$

We evaluate the expectation value in Eq. (9) using the Gutzwiller approximation [25]. This corresponds to a neglect of correlations between the two Mn impurity sites.

Due to the presence of a second Mn impurity, the point group on each Mn site is not exactly cubic. Hence, the local density matrix for the correlated orbitals

$$C_{\mathbf{g},c\sigma,c'\sigma} = \langle\Phi_0|\hat{c}^{\dagger}_{\mathbf{g},c'\sigma}\hat{c}_{\mathbf{g},c\sigma}|\Phi_0\rangle \tag{10}$$

is not diagonal. However, the nondiagonal elements are very small, of the order of 10^{-3}, and are therefore neglected in our calculations, i.e., we set

$$C_{\mathbf{g},c\sigma,c'\sigma} = \delta_{c,c'} n_{c,\sigma}. \tag{11}$$

For the same reason, we use the approximation that the matrix for the electron transfer renormalization is diagonal, $q_{c\sigma}^{c'\sigma'} = \delta_{c,c'}\delta_{\sigma,\sigma'}q_{c,\sigma}$. Then, the energy functional can be cast into the form [32]

$$\begin{aligned} E^{\mathrm{GA}}(\{\lambda_{\Gamma},|\Phi_0\rangle\}) = {}& \langle\Phi_0|\hat{T}|\Phi_0\rangle + \sum_{\mathbf{i},b,\sigma} t_{\mathbf{i},b,\sigma}^{\mathbf{i},b,\sigma}\langle\Phi_0|\hat{n}_{\mathbf{i},b\sigma}|\Phi_0\rangle \\ & + \sum_{\Gamma} E_{\Gamma}\lambda_{\Gamma}^2\langle\Phi_0|(\hat{m}_{\mathbf{f}_1,\Gamma}+\hat{m}_{\mathbf{f}_2,\Gamma})|\Phi_0\rangle \\ & - E_{\mathrm{dc}}\langle\Phi_0|\hat{n}_{\mathbf{f}_1}+\hat{n}_{\mathbf{f}_2}|\Phi_0\rangle, \end{aligned} \tag{12}$$

where

$$\hat{T} = \sum_{\mathbf{i}\neq\mathbf{j},b_1,b_2,\sigma} q_{b_1,\sigma}q_{b_2,\sigma}\left(t_{\mathbf{i},b_1,\sigma}^{\mathbf{j},b_2,\sigma}\right)^{\mathbf{f}_1,\mathbf{f}_2}\hat{c}^{\dagger}_{\mathbf{i},b_1\sigma}\hat{c}_{\mathbf{j},b_2\sigma}. \tag{13}$$

The q factors depend on the variational parameters λ_{Γ} and the local densities $n_{c,\sigma}$; explicit expressions can be found in Ref. [25]. We include the Lagrange parameter E_{SP} for the normalization of $|\Phi_0\rangle$ and $\eta_{c,\sigma}$ to fulfill Eq. (11). Then, the minimization of the energy functional (12) with respect to $\langle\Phi_0|$ leads to the effective single-particle problem [33]

$$\begin{aligned} \hat{H}_0^{\mathrm{qp}}|\Phi_0\rangle &= E_{\mathrm{SP}}|\Phi_0\rangle, \\ \hat{H}_0^{\mathrm{qp}} &= \hat{T} + \sum_{\mathbf{i},b,\sigma} t_{\mathbf{i},b,\sigma}^{\mathbf{i},b,\sigma}\hat{n}_{\mathbf{i},b\sigma} \\ &\quad - \sum_{c,\sigma}(E_{\mathrm{dc}}+\eta_{c,\sigma})\left(\hat{n}_{\mathbf{f}_1,c\sigma}+\hat{n}_{\mathbf{f}_2,c\sigma}\right). \end{aligned} \tag{14}$$

The Lagrange parameters $\eta_{c,\sigma}$ are variational parameters that control the local spin density in the $3d$ levels on the Mn ions, while the double-counting energy E_{dc} determines the average number of Mn $3d$ electrons.

C. Exchange couplings

The notion of an "exchange coupling" between the two Mn atoms hinges on the concept of a Heisenberg exchange between the two Mn impurity spins at $\mathbf{f}_1$ and $\mathbf{f}_2$

$$\hat{H}_{\mathrm{Heis}}^{\mathbf{f}_1,\mathbf{f}_2} = 2J_{\mathbf{f}_1-\mathbf{f}_2}\mathbf{S}_{\mathbf{f}_1}\cdot\mathbf{S}_{\mathbf{f}_2}. \tag{15}$$

Here, we tacitly assume that the average filling of the $3d$ shell in the Mn atoms is close to integer filling, i.e., $n_d \approx 5$, and the Hund's-rule coupling fixes the ground-state spin to $s = 5/2$ on each ion. The exchange coupling is positive, $J_{\mathbf{f}_1-\mathbf{f}_2} > 0$, for an antiferromagnetic coupling.

Under the assumption that a Heisenberg model provides an adequate description of the ground state (and low-energy excitations) of our two Mn impurities, we can estimate their exchange coupling using the band-structure and GGA+Gutzwiller approach. We orient the Mn spins into the z direction, either parallel ("ferromagnetic alignment") or antiparallel ("Neél-antiferromagnetic alignment"). The algorithm converges to the corresponding (local) minima and provides $(\Delta E)_{\mathbf{f}_1-\mathbf{f}_2} = E_{\uparrow\uparrow} - E_{\uparrow\downarrow}$ for the energy differences. This energy difference can also be calculated from the Heisenberg model (15),

$$\begin{aligned} (\Delta E)_{\mathbf{f}_1-\mathbf{f}_2} &= 2J_{\mathbf{f}_1-\mathbf{f}_2}\langle\mathrm{FM}|\mathbf{S}_{\mathbf{f}_1}\cdot\mathbf{S}_{\mathbf{f}_2}|\mathrm{FM}\rangle \\ &\quad - 2J_{\mathbf{f}_1-\mathbf{f}_2}\langle\mathrm{AFM}|\mathbf{S}_{\mathbf{f}_1}\cdot\mathbf{S}_{\mathbf{f}_2}|\mathrm{AFM}\rangle \\ &= 4J_{\mathbf{f}_1-\mathbf{f}_2}(5/2)^2 = 25J_{\mathbf{f}_1-\mathbf{f}_2}, \end{aligned} \tag{16}$$

with the spin states $|\mathrm{FM}\rangle = |5/2,5/2\rangle_{\mathbf{f}_1}|5/2,5/2\rangle_{\mathbf{f}_2}$ and $|\mathrm{AFM}\rangle = |5/2,5/2\rangle_{\mathbf{f}_1}|5/2,-5/2\rangle_{\mathbf{f}_2}$. Here we used that only the z components contribute to the expectation values. In this way, the values $J_{\mathbf{f}_1-\mathbf{f}_2} = (\Delta E_{\mathbf{f}_1-\mathbf{f}_2})/25$ are accessible from approaches that employ itinerant electrons.

Of course, the preceding statements are only valid for isolated Mn impurities. To calculate fourth-nearest-neighbor couplings we use $(\Delta E)_{\mathbf{f}_1-\mathbf{f}_2} = 50J_{\mathbf{f}_1-\mathbf{f}_2}$ because in the $L = 128$ fourth-neighbor supercell configuration described earlier, each

Mn impurity is surrounded by two equally distant Mn sites due to periodic boundary conditions.

III. RESULTS

First, we show that the experimentally observed exchange couplings for Mn ion pairs up to fourth-neighbor distance can be reproduced from scaled DFT(GGA), GGA+U, and GGA+Gutzwiller. Second, we analyze the local occupancies as obtained from GGA+Gutzwiller.

A. Exchange couplings

The values for the exchange couplings J_n in Cd(Mn)Te are known from experiment for up to fourth neighbors on the cation fcc lattice. The values for the couplings have been determined from the steps in the magnetization as a function of the externally applied field for very low temperatures, $T \lesssim 0.1\,\mathrm{K}$. Their sequence, e.g., the fact that $J_4 > J_2, J_3$, has been extracted from a fit of the data to cluster spin models. Malarenko, Jr. *et al.* [13] find $J_1 = 6.1 \pm 0.3\,\mathrm{K}$, $J_2 = 0.06 \pm 0.01\,\mathrm{K}$, $J_3 = 0.18 \pm 0.01\,\mathrm{K}$, and $J_4 = 0.39 \pm 0.02\,\mathrm{K}$. In this section we derive and compare the exchange couplings from DFT(GGA), GGA+U, and GGA+Gutzwiller calculations, and compare the resulting magnetization curves with experiment.

1. Coupling strengths

The DFT(GGA) calculation does not contain any specific parameters to adjust the exchange couplings. For large supercells, $L = 128$, the influence of Mn pairs between neighboring supercells is negligibly small.

As seen from Table I, the value for the nearest-neighbor coupling from DFT(GGA) is too large by more than a factor of 2, $J_1^{\mathrm{DFT}} = 17.1\,\mathrm{K} \approx J_1/0.36$. DFT(GGA) overestimates the size of the exchange coupling because it finds a too small charge-transfer gap Δ_{CT} between occupied Te levels and unoccupied Mn levels in Cd(Mn)Te. In superexchange models [18], the exchange integral J_1 is inversely proportional to Δ_{CT} so that the exchange integral J_1 becomes too large in DFT(LDA) and DFT(GGA), by almost a factor of 3. GGA+U is frequently used to tackle gap problems in correlated insulators. When we apply a Hubbard U on the Mn sites, we find a larger charge-transfer gap which leads to smaller exchange couplings (see below). As mentioned in Sec. II A, the gap in pure CdTe is too small in DFT(GGA) calculations. This can also be corrected using GGA+U [29]. However, the exchange couplings between Mn ions are mediated by electron transfer processes between Mn and Te so that the precise value of the CdTe band gap is irrelevant for our considerations.

TABLE I. Heisenberg exchange couplings J_n in K between Mn ions at nth-neighbor distance on the Cd fcc lattice in CdTe from experiment [13], and from DFT(GGA), DFT(GGA) scaled by a factor $s = 0.357$, GGA+U for $\overline{U} = U - J = 2.65\,\mathrm{eV}$, and GGA+Gutzwiller for $A = 4.4\,\mathrm{eV}$, $B = 0.1\,\mathrm{eV}$, $C = 0.4\,\mathrm{eV}$, and $n_d = 5.19$.

J^{CdTe}	Exp.	GGA	s · GGA	GGA+U	GGA+G
J_1	6.1	17.1	6.1	6.1	6.1
J_2	0.06	0.30	0.11	0.10	0.10
J_3	0.18	0.96	0.34	0.30	0.27
J_4	0.39	1.44	0.51	0.49	0.61

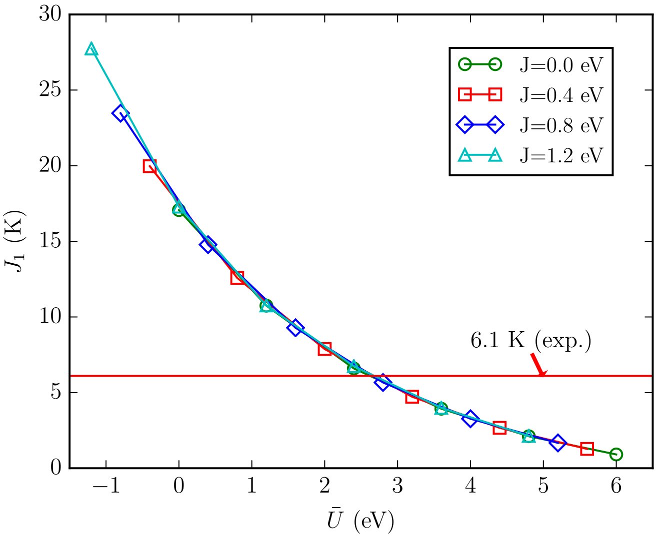

FIG. 3. Heisenberg exchange coupling J_1 between two Mn ions in CdTe at nearest-neighbor distance from GGA+U as a function of $\overline{U} = U - J$ calculated for a supercell with $L = 128$ atoms using the FLEUR program package. The red horizontal line shows the experimental value $J_1^{\mathrm{exp}} = 6.1\,\mathrm{K}$.

In Fig. 3 we show the dependence of $J_1^{\mathrm{GGA}+U}$ as a function of U for various values of J. The exchange coupling only depends on the combination $\overline{U} = U - J$ [34], where U and J are a measure for the intra-atomic Coulomb and exchange interaction, respectively. For $\overline{U} = 2.65\,\mathrm{eV}$ we obtain $J_1^{\mathrm{GGA}+\overline{U}} = 6.1\,\mathrm{K}$. The values for other exchange interactions for farther distances are collected in Table I. The values for $J_{2,3,4}^{\mathrm{GGA}+U}$ are very similar, and even slightly closer to experiment, than those from the scaled DFT(GGA). This demonstrates that an adjustment of the charge-transfer gap cures in effect the overestimation of the exchange interactions in DFT(GGA).

Lastly, we discuss the results for J_n as obtained from our GGA+Gutzwiller calculations. We set $C = 0.4\,\mathrm{eV}$, in agreement with crystal-field theory for data from infrared spectroscopy for isolated Mn^{2+} ions in CdTe [2]. Moreover, we use $C = 4B$, i.e., $B = 0.1\,\mathrm{eV}$, as is a reasonable assumption for transition metals [35]. A similar set of values was used in a recent study of exchange integrals in Mn-doped II-VI semiconductors [18]. The Hubbard-parameter U in transition metals is of the order of several eV [36]. In this work we set $A = 4.4\,\mathrm{eV}$. Note that we have $U = A + 4B + 3C$ and $J = (5/2)B + C$ for our intraorbital Hubbard interaction and Hund's-rule coupling, or, for the Slater-Condon parameters, we have $F^{(0)} = A + (7/5)C$, $F^{(2)} = 49B + 7C$, and $F^{(4)} = (63/5)C$ [37]. Therefore, our Hund's-rule exchange on the Mn sites is $J = 0.65\,\mathrm{eV}$ and we employ $F^{(0)} = 4.96\,\mathrm{eV}$ or $U = 6\,\mathrm{eV}$.

In Fig. 4, we show J_1 as a function of the electron number n_d in the Mn 3d shell. As seen from the figure, the curves for $4.0 \leqslant A \leqslant 4.8\,\mathrm{eV}$ and $0.3 \leqslant C \leqslant 0.5\,\mathrm{eV}$ essentially collapse onto each other in the region of interest, $J_1 = 6.1\,\mathrm{K}$. Therefore,

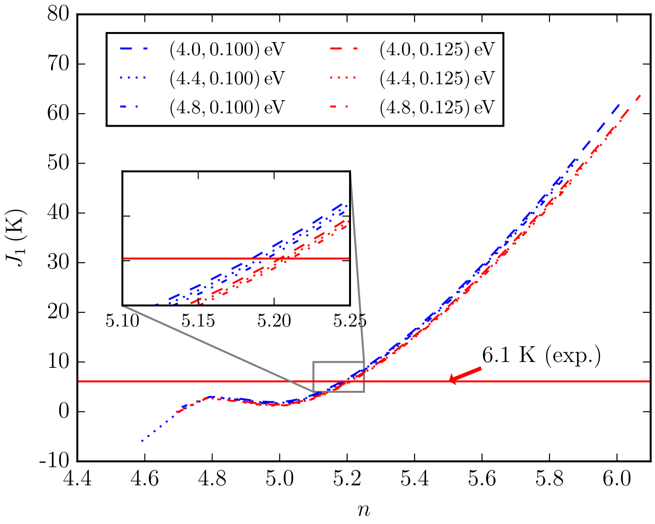

FIG. 4. Heisenberg exchange coupling J_1 between two Mn ions in CdTe at nearest-neighbor distance from GGA+Gutzwiller as a function of the number of electrons in the Mn $3d$ shell for various values of the Racah parameters A, B, and $C = 4B$. The red horizontal line shows the experimental value, $J_1^{\rm exp} = 6.1$ K.

the specific choice of the Racah parameters is not crucial. As also seen from Fig. 4, the filling is not integer. Instead, we find that $n_d = 5.19$ reproduces the nearest-neighbor Heisenberg exchange coupling best for $A = 4.4$ eV, $B = 0.1$ eV, $C = 0.4$ eV. The resulting values for the exchange couplings for Mn ions in CdTe are compiled in Table I.

Our Gutzwiller calculations here are very close to a Hartree-Fock calculation because the Gutzwiller wave function reduces to a Hartree-Fock wave function near half filling and for strong spin polarization. Correlation effects are small for the two fully polarized Mn atoms with their (anti-)parallel spins. We discuss this point further in Sec. III B. This agreement is specific for Mn in II-VI semiconductors because we encounter a fully polarized, half-filled $3d$ shell in a wide-gap insulator. In other systems, correlation effects are more pronounced, as seen in some preliminary calculations for Cr-doped CdTe or Mn-doped GaAs.

For future reference, we compile the exchange couplings for Zn(Mn)Se, Zn(Mn)Te, and Zn(Mn)S in Table II. Note that the exchange couplings for $n > 4$ are at least an order of magnitude smaller than J_2, J_3, of the order of $J_{n\geqslant 5} = 0.01$ K, or less. This justifies our restriction to $J_{n\leqslant 4}$.

As seen from the table, the GGA+Gutzwiller method overestimates by some 20–30% the nearest-neighbor exchange couplings J_1 for Zn-VI semiconductors (VI=Te, Se, S) when we use $A = 4.4$ eV, $B = 0.1$ eV, $C = 0.4$ eV, and $n_d = 5.19$ for the Mn ions. With this parameter set, the method can be used to provide a reasonable estimate for the nearest-neighbor couplings for Mn ion pairs in II-VI semiconductors. GGA+Gutzwiller provides a much better estimate for the couplings $J_{n\geqslant 2}$ than DFT(GGA) but they are still systematically too large by a factor 2 to 3.

2. *Magnetization for small doping and low temperatures*

As an application, we calculate the magnetization $M(B)$ as a function of the applied external field B for $\mathrm{Cd}_{1-x}\mathrm{Mn}_x\mathrm{Te}$ at small but finite doping $x = 0.005$. A Mn ion is placed in the center of a large but finite fcc lattice with 50^3 sites. Then, Cd atoms in the surrounding of the "seed site" are replaced by Mn atoms with probability x. As a first possibility, the central Mn ion remains isolated, i.e., with only Cd atoms on its first-, second-, third-, and fourth-neighbor shell ("maximal surrounding"). In the absence of spin-orbit coupling, the spin of such an isolated Mn ion aligns with any finite magnetic field so that its magnetic response is given by the Brillouin function. Note that neglecting the spin-orbit coupling is justified because of the full magnetic polarization of the Mn ions [38].

TABLE II. Heisenberg exchange couplings J_n in K between Mn ions at nth-neighbor distance on the cation fcc lattice in ZnTe, ZnSe, and ZnS from experiment [13], from (scaled) DFT(GGA), and from GGA+Gutzwiller for $A = 4.4$ eV, $B = 0.1$ eV, $C = 0.4$ eV, and $n_d = 5.19$.

$J^{\rm ZnTe}$	Exp.	GGA	s · GGA	GGA+G
J_1	9.0	41.2	9.0	11.45
J_2	0.20	0.96	0.21	0.49
J_3	0.16	2.61	0.57	0.54
J_4	0.51	3.97	0.87	1.13
$J^{\rm ZnSe}$	Exp.	GGA	s · GGA	GGA+G
J_1	12.2	48.1	12.2	14.97
J_2	0.16	0.81	0.21	0.28
J_3	0.07	1.61	0.41	0.42
J_4	0.43	3.26	0.82	1.16
$J^{\rm ZnS}$	Exp.	GGA	s · GGA	GGA+G
J_1	16.9	60.3	16.9	19.73
J_2	0.27	0.99	0.28	0.47
J_3	0.04	1.14	0.32	0.40
J_4	0.41	2.85	0.80	0.97

A second possibility are two-spin clusters with exactly one Mn ion in the maximal surrounding of the seed site. Two such clusters are equivalent when they can be mapped onto each other by applying some space-group transformations of the fcc lattice. Since equivalent clusters lead to the same magnetic response we only need to store one representative C and determine its multiplicity A_C. Moreover, we need to calculate the probability p_C that a lattice point is part of cluster C [12,39]. For example, for a nearest-neighbor cluster we have $A_C = 12$ and $p_C = x^2(1-x)^{72}$ (because in this case 72 sites must be unoccupied). This construction principle is readily generalized for clusters with three or more spins.

In this paper we include clusters with one to four Mn atoms and thus find in total 1130 inequivalent clusters C. At doping $x = 0.005$, clusters with up to three Mn atoms cover 98.5% of all possible configurations, and clusters with up to four Mn atoms cover 99.6% of all possible configurations. Therefore, clusters with five and more Mn atoms are irrelevant at $x = 0.005$.

For each cluster C, the interaction between the Mn spins is described by a Heisenberg model,

$$\hat{H}^C_{\rm Heis}(B) = \sum_{\mathbf{f}_1,\mathbf{f}_2\,\in\, C\$\mathbf{f}_1 \neq \mathbf{f}_2)} J_{\mathbf{f}_1-\mathbf{f}_2}\hat{\mathbf{S}}_{\mathbf{f}_1}\cdot\hat{\mathbf{S}}_{\mathbf{f}_2} - g\mu_{\rm B}B\sum_{\mathbf{f}\in C}\hat{S}^z_{\mathbf{f}}, \tag{17}$$

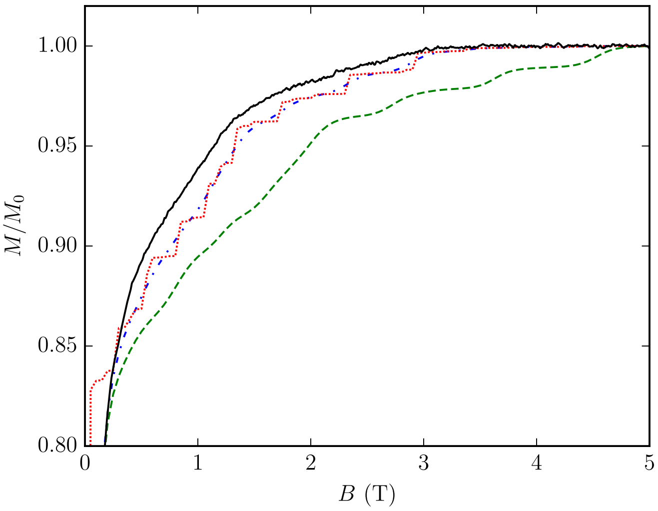

FIG. 5. Magnetization $M(B)$ as a function of the external field B normalized to its value at $B = 5$ T for $\mathrm{Cd}_{1-x}\mathrm{Mn}_x\mathrm{Te}$ at Mn doping $x = 0.005$. Black line (solid), experimental curve [13]; red line (dotted), Heisenberg model with experimental coupling parameters at $T = 0$; blue line (dash-dotted), Heisenberg model with experimental coupling parameters at $T_{\mathrm{spin}} = 0.1$ K; green line (dashed), Heisenberg model with GGA+Gutzwiller parameters at $T_{\mathrm{spin}} = 0.1$ K. Clusters with up to four Mn ions are included.

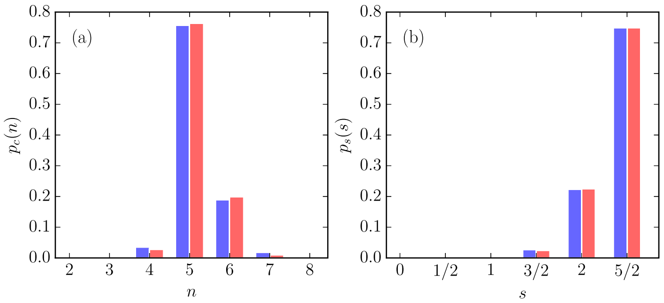

FIG. 6. (a) Mn charge distribution $p_c(n)$ as a function of the number n of $3d$ electrons and (b) Mn spin distribution $p_s(s)$ as a function of the spin s of $3d$ electrons for $A = 4.4$ eV, $B = 0.1$ eV, $C = 0.4$ eV, and $n_d = 5.19$ in GGA+Gutzwiller (red columns), in comparison with the Hartree–Fock result (blue columns).

where the sums run over all lattice sites $\mathbf{f}$ in cluster C, containing $n_C = 1 \ldots 4$ spins. We include the interaction with the external field B where $g = 2$ is the gyromagnetic ratio and μ_{B} is the Bohr magneton. For our comparisons with experiment, we use the experimental values for J_n from Table I and theoretical values from the GGA+Gutzwiller approach. However, the differences between scaled GGA, GGA+U, and GGA+Gutzwiller are fairly small.

For each cluster C, we determine its contribution to the magnetization per lattice site,

$$M^C(B) = \frac{1}{n_C}\mathrm{Tr}\left(\hat{\rho}_C \sum_{\mathbf{f}\in C} \hat{S}^z_{\mathbf{f}}\right), \quad \hat{\rho}_C = \frac{e^{-\beta \hat{H}^C_{\mathrm{Heis}}(B)}}{\mathrm{Tr}\left(e^{-\beta \hat{H}^C_{\mathrm{Heis}}(B)}\right)} \tag{18}$$

with $\beta = 1/(k_{\mathrm{B}} T_{\mathrm{spin}})$. The trace is readily calculated using the exact spectrum that we obtain from a complete diagonalization of the cluster Hamiltonian $\hat{H}^C_{\mathrm{Heis}}(B)$. The magnetization per lattice site is then given by the sum over all clusters weighted by their multiplicity A_C and probability p_C:

$$M(B) = \sum_C A_C p_C M^C(B). \tag{19}$$

We show the resulting magnetization in Fig. 5.

The curve for zero temperature shows the expected magnetization steps that occur when more and more Mn pairs (or clusters) align with the external field [11]. When we use the experimentally determined values for the exchange couplings from Table I and a spin temperature $T_{\mathrm{spin}} = 100$ mK that is somewhat higher than the environment temperature $T = 20$ mK [13], we find that the agreement between theory and experiment for $M(B)$ is very good. The agreement becomes slightly worse when we use the coupling parameters calculated by GGA+Gutzwiller. Note that the experimentally accessible magnetic fields probe mostly J_2, J_3, and J_4 because we have $k_{\mathrm{B}}T, g\mu_{\mathrm{B}}B \ll J_1$ and $k_{\mathrm{B}}T, g\mu_{\mathrm{B}}B \gg J_{n\geqslant 5}$.

B. Density and spin distributions

To gain further insight into the nature of the ground state of the Mn ion, we present results for the local occupancies which can be calculated from the Gutzwiller variational parameters in the ground state [40].

We start our discussion with the probability distribution $p_c(n)$ to find n $3d$ electrons on the Mn ion on site $\mathbf{f}$ ($0 \leqslant n \leqslant 10$). As seen from Fig. 6(a) the distribution peaks at $n = 5$, which reflects the fact that the average particle number is $n_d = 5.19$ (see Sec. III A 1). Correspondingly, there also is a sizable probability to find $3d^6$ configurations on the Mn ion whereas the probability for all other occupation numbers is negligible. Note that this distribution is not the result of electronic correlations because the corresponding Hartree-Fock state displays almost the same distribution function.

The probability distribution function $p_s(s)$ for finding local spins with size $0 \leqslant s \leqslant 5/2$ is very similar to the distribution in the single-particle product state $|\Phi_0\rangle$, i.e., the correlation enhancement of the local spin moment is also small for the spin distribution function [see Fig. 6(b)]. The average local spin is $\langle \hat{S}^z_{\mathbf{f}} \rangle_{\mathrm{loc}} = 2.33$ because the admixture of spin $s = 2$ to the dominant configurations with $s = 5/2$ is not negligibly small.

The Mn ions do not show integer filling $n_d = 5$, nor does the spin moment correspond to the atomic spin $s = 5/2$. This observation puts into question the concept of a Heisenberg-model description that we employed in Sec. II C to derive the exchange couplings. Even if we accept a noninteger filling of the Mn ions' $3d$ shell, we are actually far from a local-moment regime that is implicit in the Heisenberg-model description (15) in Sec. II C. This issue can be resolved as seen in the next section.

IV. MAGNETIC RESPONSE OF ION PAIRS AT NONINTEGER FILLING

In order to reconcile the finding of a noninteger Mn $3d$ filling and the notion of a spin $s = 5/2$ effective Heisenberg model, we study the magnetic response in a simplified toy

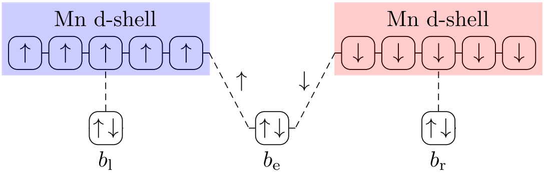

FIG. 7. Toy model for the study of two Mn atoms with two reservoir sites and an indirect Mn-Mn coupling via a charge-transfer site.

model of two Mn atoms close to their Hund's-rule ground states that are coupled to three uncorrelated sites. The uncorrelated sites serve two purposes, namely, (i) they act as a reservoir to adjust the average particle number on the Mn sites away from integer filling and (ii) they serve as an intermediate charge-transfer (exchange) site to mimic the super-exchange mechanism.

A. Model Hamiltonian

The Hamiltonian for our few-site toy model, illustrated in Fig. 7, is readily formulated. We use the local Hamiltonian $\hat{H}^{\mathrm{loc}}_{\mathbf{g}}$ defined in Eq. (6) for the Mn atoms at $\mathbf{f}_\mathrm{l}$ and $\mathbf{f}_\mathrm{r}$, and

$$\hat{H}^{\mathrm{loc}}_{\mathrm{j}} = \epsilon_\mathrm{j} \sum_{\sigma} \hat{n}_{\mathrm{j},\sigma}, \tag{20}$$

for the local Hamiltonians of the three uncorrelated orbitals. Here, ϵ_j (j = l,e,r) are the local chemical potentials that permit the adjustment of the average electron number in the left (l) and right (r) bath orbitals and the exchange (e) orbital, and $\hat{n}_{\mathrm{j},\sigma} = \hat{c}^\dagger_{\mathrm{j},\sigma}\hat{c}_{\mathrm{j},\sigma}$ counts the number of electrons in the uncorrelated orbitals. The sites are coupled via the kinetic terms

$$\begin{aligned}\hat{T}_{\mathrm{l/e},\mathbf{f}_\mathrm{l}} &= \sum_{c,\sigma} T^{\mathrm{l/e},\sigma}_{\mathbf{f}_\mathrm{l},c,\sigma}\hat{c}^\dagger_{\mathbf{f}_\mathrm{l},c\sigma}\hat{c}_{\mathrm{l/e},\sigma} + \mathrm{H.c.},\\ \hat{T}_{\mathrm{e/r},\mathbf{f}_\mathrm{r}} &= \sum_{c,\sigma} T^{\mathrm{e/r},\sigma}_{\mathbf{f}_\mathrm{r},c,\sigma}\hat{c}^\dagger_{\mathbf{f}_\mathrm{r},c\sigma}\hat{c}_{\mathrm{e/r},\sigma} + \mathrm{H.c.}\end{aligned} \tag{21}$$

The full model Hamiltonian reads

$$\begin{aligned}\hat{H} = {}& \hat{H}^{\mathrm{loc}}_{\mathbf{f}_\mathrm{l}} + \hat{H}^{\mathrm{loc}}_{\mathbf{f}_\mathrm{r}} + \hat{H}^{\mathrm{loc}}_{\mathrm{l}} + \hat{H}^{\mathrm{loc}}_{\mathrm{e}} + \hat{H}^{\mathrm{loc}}_{\mathrm{r}}\\ &+ \hat{T}_{\mathrm{l},\mathbf{f}_\mathrm{l}} + \hat{T}_{\mathrm{e},\mathbf{f}_\mathrm{l}} + \hat{T}_{\mathrm{e},\mathbf{f}_\mathrm{r}} + \hat{T}_{\mathrm{r},\mathbf{f}_\mathrm{r}}.\end{aligned} \tag{22}$$

The maximal dimension of the corresponding Fock space is $\dim H = 1024^2 \times 4^3$. It is too large to be handled exactly.

From our analysis in Sec. III we know that, for large U, J, those Mn configurations are dominantly occupied that, in the sectors with $n_d = 4{,}5{,}6$ electrons, have maximal spin $s_{\max} = 2{,}5/2{,}2$ and maximal orbital momentum $l_{\max} = 2{,}0{,}2$, which is a good quantum number in spherical approximation. Therefore, we restrict the Hilbert space of our two Mn atoms to these atomic subspaces. To this end, we introduce the projection operators $\mathcal{P}^{\mathrm{H}}_{\mathbf{g},n_d}$ onto the lowest-lying $(2s_{\max}+1)(2l_{\max}+1)$ Hund's-rule states for fixed electron number n_d

$$\begin{aligned}\hat{H}^{\mathrm{loc}}_{\mathbf{g}}|\Gamma_n\rangle_{\mathbf{g}} &= E^{\mathrm{loc}}_n|\Gamma_n\rangle_{\mathbf{g}},\\ \hat{n}_{\mathbf{g}}|\Gamma_n\rangle_{\mathbf{g}} &= n_d|\Gamma_n\rangle_{\mathbf{g}},\\ \hat{\mathbf{S}}^2_{\mathbf{g}}|\Gamma_n\rangle_{\mathbf{g}} &= s_{\max}(s_{\max}+1)|\Gamma_n\rangle_{\mathbf{g}},\\ \hat{\mathbf{L}}^2_{\mathbf{g}}|\Gamma_n\rangle_{\mathbf{g}} &= l_{\max}(l_{\max}+1)|\Gamma_n\rangle_{\mathbf{g}},\\ \mathcal{P}^{\mathrm{H}}_{\mathbf{g},n_d} &= \sum_{\Gamma_n}|\Gamma_n\rangle_{\mathbf{g}}\,{}_{\mathbf{g}}\langle\Gamma_n|\,.\end{aligned} \tag{23}$$

Then, we define the total projection operator

$$\mathcal{P}^{\mathrm{H}}_{4,5,6} = \left(\sum_{n_d=4}^{6}\mathcal{P}^{\mathrm{H}}_{\mathbf{f}_\mathrm{l},n_d}\right)\left(\sum_{n_d=4}^{6}\mathcal{P}^{\mathrm{H}}_{\mathbf{f}_\mathrm{r},n_d}\right), \tag{24}$$

and we limit ourselves to the investigation of our model Hamiltonians in the projected form

$$\mathcal{H} = \mathcal{P}^{\mathrm{H}}_{4,5,6}\hat{H}\mathcal{P}^{\mathrm{H}}_{4,5,6}. \tag{25}$$

The dimension of the partial Fock space on the Mn atoms is $(2s_{\max}+1)(2l_{\max}+1)$ so that the maximal Fock-space dimension is $\dim\mathcal{H} = (25+6+25)^2 \times 4^3 = 200\,704$. This partial Fock space is accessible using the Lanczos technique.

B. Magnetization plateaus

The magnetic field couples to the spin component of the Mn atoms in the z direction

$$\hat{H}_B = -g\mu_\mathrm{B}B\big(\hat{S}^z_{\mathbf{f}_\mathrm{l}} + \hat{S}^z_{\mathbf{f}_\mathrm{r}}\big). \tag{26}$$

The magnetization is obtained from

$$M(B) = \langle\Psi_0|\hat{S}^z_{\mathbf{f}_\mathrm{l}} + \hat{S}^z_{\mathbf{f}_\mathrm{r}}|\Psi_0\rangle, \tag{27}$$

where $|\Psi_0\rangle$ is the ground state of our model Hamiltonian in the presence of a magnetic field

$$\mathcal{H}(B) = \mathcal{H} + \hat{H}_B. \tag{28}$$

We employ the Lanczos algorithm to find $|\Psi_0(B)\rangle$.

We fix the total number of electrons in the system to $n_{\mathrm{tot}} = 16$, and choose the local chemical potentials $\epsilon_\mathrm{l} = \epsilon_\mathrm{r}$ to adjust the average electron number on the Mn sites so that we have an average number of $n_d = 5.30$ electrons. Note that this number marginally changes as a function of the magnetic field. We set all electron transfer matrices equal in Eq. (21), $T^{\cdot\cdot}_{\cdot\cdot} = 1\,\mathrm{eV}$.

In the following case (i), we set $\epsilon_\mathrm{e} = 8.0\,\mathrm{eV}$ and $\epsilon_{\mathrm{l,r}} = 23.1\,\mathrm{eV}$ so that we have $n_\mathrm{e} = 1.98$ electrons in the exchange orbital and $n_{\mathrm{l,r}} = 1.71$ electrons in each bath orbital in the ground state. The resulting magnetization steps are equidistant, as shown in Fig. 8(a), despite the fact that the Mn filling is far from integer.

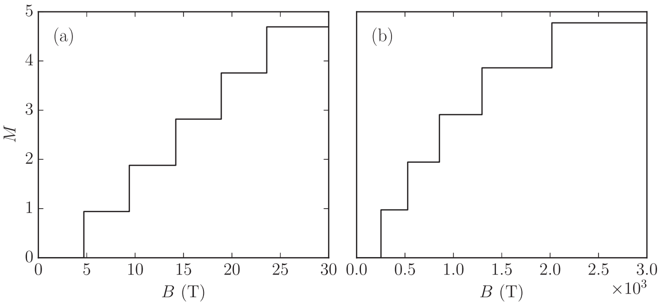

FIG. 8. Magnetization $M(B)$ as a function of the external field for the toy model with (a) an almost filled exchange site, $n_\mathrm{e} = 1.98$, and (b) a partly filled exchange site, $n_\mathrm{e} = 1.51$.

The width of the magnetization steps become nonuniform in case (ii) when the exchange site is not almost filled. To illustrate this case, we choose $\epsilon_{\rm e} = 22.6$ eV and $\epsilon_{1,\rm r} = 19.5$ eV so that we have $n_{1,\rm r} = 1.93$ electrons in each bath orbital and $n_{\rm e} = 1.51$ electrons in the exchange orbital. Now, the lengths of the corresponding magnetization plateaus are inequivalent, as shown in Fig. 8(b).

The toy model shows that equidistant plateaus are possible even though the occupation of the Mn sites is not integer. Our numerical observations can be readily understood using perturbative arguments. For negligible couplings to the exchange orbital, the ground state of each Mn ion and its attached bath site has spin $s = 5/2$. Note that this spin is not solely located on the Mn site but also partly on the corresponding bath site. In case (i), the exchange orbital introduces only a small coupling between the left and the right spin-5/2 systems, and perturbation theory leads to a dominant term of the usual antiferromagnetic Heisenberg form (15). Consequently, the magnetization steps are equidistant [10,11]. In case (ii), charge fluctuation contributions invalidate the simple spin-only picture. This results in nonequidistant magnetization steps as seen in Fig. 8(b).

When we apply the Gutzwiller approximation scheme used in Sec. III to case (i) of our toy model, we find an exchange coupling J_1 that is very close to the exact value derived from the width of the magnetization plateaus. This corroborates our finding in Sec. III and further justifies the applicability of our toy model.

Due to the large gap for charge excitations, the situation of Mn ions in CdTe resembles scenario (i) in our toy model and explains the experimental observation of equidistant magnetization plateaus. The filling of the Mn 3*d* shell is not integer but the total spin of the Mn ion and its surrounding atoms still is essentially $s = 5/2$.

V. CONCLUSIONS

In this paper we used three band-structure methods, DFT(GGA), GGA+U, and GGA+Gutzwiller, to derive the exchange couplings between Mn ions diluted in II-VI semiconductor host materials such as CdTe. First, we calculate the energy of the configurations with parallel and antiparallel alignments of the Mn spins. Next, we interpret the energy difference in terms of a two-spin Heisenberg model and thereby deduce the exchange couplings as a function of the Mn-Mn separation for up to fourth-neighbor distances.

For the GGA calculations we employ the FLEUR code with the functional of Perdew, Burke, and Ernzerhof for large supercells with $L = 128$ atoms where two of the Cd ions are replaced by isovalent Mn ions. The *ab initio* results for the exchange couplings are too large by a factor of 2 to 3, which is related to the fact that DFT(GGA) underestimates gaps in II-VI semiconductors systematically. The nearest-neighbor couplings J_1 for Mn ions in II-VI semiconductors can be reconciled with experiment by using the GGA+U and GGA+Gutzwiller methods. These methods employ adjustable parameters that are used to match the experimental value for J_1 in Cd(Mn)Te. The exchange couplings $J_{2,3,4}$ for second-, third-, and fourth-neighbor distances are then predictions from theory.

In general, the values for $J_{n\geqslant 2}$ agree qualitatively with experiment, i.e., band theory recovers $J_4 > J_2, J_3$ and $J_{n\geqslant 5} \lesssim 0.01$ K. However, the values for the couplings do not agree perfectly, i.e., we observe quantitative deviations up to a factor of 2. About the same level of accuracy can be obtained by a simple rescaling of the DFT(GGA) data that fits the nearest-neighbor coupling J_1 (see table II). The bare energy scale in our itinerant-electron description is of the order of several eV, i.e., of the order of 10^5 K, whereas the exchange couplings $J_{n\geqslant 2}$ are 1 K and below. Therefore, it does not come as a surprise that the band-structure methods reach their accuracy limits.

The notion of exchange couplings and the applicability of the superexchange approach hinge on the mapping of the low-energy degrees of freedom of the itinerant-electron problem to those of a spin-5/2 Heisenberg model. This mapping successfully explains the equidistant magnetization plateaus as a function of applied magnetic field, as seen in experiment. However, the analysis of the Gutzwiller ground state for the two-ion Hubbard model shows that the filling of the Mn 3*d* shell is *not* integer, which seemingly invalidates the whole concept of localized spins. The analysis of an exactly solvable few-site toy model reassures that an integer filling is not a prerequisite for equidistant magnetization plateaus. Due to the hybridization of the Mn 3*d* orbitals with its insulating environment, a slightly delocalized spin-5/2 magnetic moment is formed combing Mn $3d^5$ and $3d^6$ with neighboring valence-band states. Our picture of an extended spin-5/2 magnetic moment interacting with each other reconciles the usage of an effective spin-5/2 Heisenberg model to explain the experimentally observed magnetization steps and simultaneously a noninteger valence of the Mn 3*d* shell.

In the case of Mn-doped II-VI semiconductors, the Gutzwiller method and the Hartree-Fock approach to the two-ion Hubbard model lead to essentially the same results for an (anti-)ferromagnetic alignment of the Mn spins. Our preliminary investigations show that this is not the case for Cr in CdTe where the dopant electrons are more itinerant than in the case of Mn doping. We observe the same trend for Mn doping of GaAs and other III-V semiconductors. This observation also indicates that the Heisenberg mapping is less appropriate in these cases, and it is advisable to employ a correlated-electron approach for the description of the magnetic response in GaAs samples at low Mn doping.

In summary, we improve the understanding of exchange couplings between Mn ions in CdTe: (i) we provide an *ab initio* calculation of these parameters (beyond nearest neighbors), and (ii) we reconcile the commonly used effective Heisenberg spin models with microscopic calculations which indicate noninteger fillings at the sites of the magnetic atoms.

ACKNOWLEDGMENTS

We thank Prof. Valdir Bindilatti for providing us with his original magnetization data for Cd(Mn)Te [13], shown in Fig. 5. We also have profited from fruitful discussions with M. Bayer and D. Yakovlev. We are particularly indebted to Stefan Blügel for information on the FLEUR program and for bringing some special aspects of DFT+U to our attention. Finally, we thank the late Werner Weber who has initiated this project. Some of us (T.L., U.L., and F.B.A.) acknowledge financial support by the Deutsche Forschungsgemeinschaft and the Russian Foundation of Basic Research in the framework of the ICRC TRR 160. The authors gratefully acknowledge the computing time granted by the John-von-Neumann Institute for Computing, and provided on the supercomputer JURECA at Jülich Supercomputing Centre under Project No. HDO08.

---

[1] J. K. Furdyna, J. Appl. Phys. **64**, R29 (1988).
[2] M. Jain, *Diluted Magnetic Semiconductors* (World Scientific, Singapore, 1991).
[3] *Introduction to the Physics of Diluted Magnetic Semiconductors*, edited by J. Kossut and J. A. Gaj (Springer, Heidelberg, 2010).
[4] J. Debus, V. Y. Ivanov, S. M. Ryabchenko, D. R. Yakovlev, A. A. Maksimov, Y. G. Semenov, D. Braukmann, J. Rautert, U. Löw, M. Godlewski *et al.*, Phys. Rev. B **93**, 195307 (2016).
[5] A. A. Maksimov, D. R. Yakovlev, J. Debus, I. I. Tartakovskii, A. Waag, G. Karczewski, T. Wojtowicz, J. Kossut, and M. Bayer, Phys. Rev. B **82**, 035211 (2010).
[6] *Semiconductor Spintronics and Quantum Computation*, edited by D. D. Awschalom, D. Loss, and N. Samarth (Springer, Berlin, 2002).
[7] T. Dietl, H. Ohno, F. Matsukura, J. Cibert, and D. Ferrand, Science **287**, 1019 (2000).
[8] T. Dietl and H. Ohno, Rev. Mod. Phys. **86**, 187 (2014).
[9] T. Schäpers, *Semiconductor Spintronics* (De Gruyter, Berlin, 2016).
[10] B. E. Larson, K. C. Hass, and R. L. Aggarwal, Phys. Rev. B **33**, 1789 (1986).
[11] S. Foner, Y. Shapira, D. Heiman, P. Becla, R. Kershaw, K. Dwight, and A. Wold, Phys. Rev. B **39**, 11793 (1989).
[12] V. Bindilatti, E. ter Haar, N. F. Oliveira, Y. Shapira, and M. T. Liu, Phys. Rev. Lett. **80**, 5425 (1998).
[13] H. Malarenko, Jr., V. Bindilatti, N. F. Oliveira, Jr., M. T. Liu, Y. Shapira, and L. Puech, Physica B: Condens. Matter **284-288**, 1523 (2000).
[14] H. Bednarski, J. Cisowski, and J. Portal, J. Magn. Magn. Mater. **261**, 172 (2003).
[15] J. Spałek, A. Lewicki, Z. Tarnawski, J. K. Furdyna, R. R. Galazka, and Z. Obuszko, Phys. Rev. B **33**, 3407 (1986).
[16] B. E. Larson, K. C. Hass, H. Ehrenreich, and A. E. Carlsson, Phys. Rev. B **37**, 4137 (1988).
[17] S. Barthel, G. Czycholl, and G. Bouzerar, Eur. Phys. J. B **86**, 11 (2013).
[18] A. Savoyant, S. D'Ambrosio, R. O. Kuzian, A. M. Daré, and A. Stepanov, Phys. Rev. B **90**, 075205 (2014).
[19] T. Chanier, F. Virot, and R. Hayn, Phys. Rev. B **79**, 205204 (2009).
[20] T. Chanier, F. Virot, and R. Hayn, Phys. Rev. B **83**, 239903 (2011).
[21] J. P. Perdew, K. Burke, and M. Ernzerhof, Phys. Rev. Lett. **77**, 3865 (1996).
[22] FLEUR, The Jülich FLAPW code family, http://www.flapw.de/, accessed: Feb. 2015.
[23] N. W. Ashcroft and N. D. Mermin, *Solid State Physics*, 34th ed. (Brooks/Cole, Belmont, 2008).
[24] V. I. Anisimov, F. Aryasetiawan, and A. I. Lichtenstein, J. Phys.: Condens. Matter **9**, 767 (1997).
[25] T. Schickling, J. Bünemann, F. Gebhard, and W. Weber, New J. Phys. **16**, 093034 (2014).
[26] K. M. Ho, J. Schmalian, and C. Z. Wang, Phys. Rev. B **77**, 073101 (2008).
[27] X. Y. Deng, L. Wang, X. Dai, and Z. Fang, Phys. Rev. B **79**, 075114 (2009).
[28] A. A. Mostofi, J. R. Yates, Y.-S. Lee, I. Souza, D. Vanderbilt, and N. Marzari, Comput. Phys. Commun. **178**, 685 (2008).
[29] Y. Wu, G. Chen, Y. Zhu, W.-J. Yin, Y. Yan, M. Al-Jassim, and S. J. Pennycook, Comput. Mater. Sci. **98**, 18 (2015).
[30] D. G. Thomas, J. Appl. Phys. **32**, 2298 (1961).
[31] R. J. Elliott, J. A. Krumhansl, and P. L. Leath, Rev. Mod. Phys. **46**, 465 (1974).
[32] J. Bünemann, W. Weber, and F. Gebhard, Phys. Rev. B **57**, 6896 (1998).
[33] J. Bünemann, F. Gebhard, T. Schickling, and W. Weber, Phys. Status Solidi B **249**, 1282 (2012).
[34] S. L. Dudarev, G. A. Botton, S. Y. Savrasov, C. J. Humphreys, and A. P. Sutton, Phys. Rev. B **57**, 1505 (1998).
[35] S. Sugano, Y. Tanabe, and H. Kamimura, *Multiplets of Transition-Metal Ions in Crystals* (Academic, New York, 1970).
[36] F. Aryasetiawan, K. Karlsson, O. Jepsen, and U. Schönberger, Phys. Rev. B **74**, 125106 (2006).
[37] T. Schickling, J. Bünemann, F. Gebhard, and L. Boeri, Phys. Rev. B **93**, 205151 (2016).
[38] J. Bünemann, T. Linneweber, U. Löw, F. B. Anders, and F. Gebhard, Phys. Rev. B **94**, 035116 (2016).
[39] M. T. Liu, Y. Shapira, E. ter Haar, V. Bindilatti, and E. J. McNiff, Jr., Phys. Rev. B **54**, 6457 (1996).
[40] T. Schickling, F. Gebhard, J. Bünemann, L. Boeri, O. K. Andersen, and W. Weber, Phys. Rev. Lett. **108**, 036406 (2012).